technologies

MDPI

*Article*

# A Realistic Breast Phantom for Investigating the Features of the Microwave Radiometry Method Using Mathematical and Physical Modelling

**Maxim V. Polyakov** *,† **and Danila S. Sirotin** *,†

Department of Information Systems and Computer Modelling, Volgograd State University, Universitetsky pr., 100, Volgograd 400062, Russia

* Correspondence: m.v.polyakov@volsu.ru (M.V.P.); d.sirotin@volsu.ru (D.S.S.)

† These authors contributed equally to this work.

**Abstract:** This article presents the development of an anatomical breast phantom for investigating the capabilities of microwave radiometry in assessing thermal processes in biological tissues. The phantom accounts for the heterogeneous tissue structure and haemodynamics, enabling realistic heat transfer modelling. Numerical simulation software was developed, accurately reproducing experimental results and allowing the study of thermal anomalies. Experimental validation demonstrated that the temperature in the subcutaneous layer differed on average by 0.3 °C from deeper tissues, confirming the method's effectiveness. The presence of a tumour in the model resulted in a local temperature increase of up to 0.77 °C, highlighting the sensitivity of microwave radiometry to tumour-induced thermal anomalies. These findings contribute to enhancing non-invasive techniques for early breast disease detection.

**Keywords:** microwave radiometry; breast phantom; physical modelling; mathematical modelling; temperature fields; thermal processes; bioheat transfer; biological tissues

check for updates

Academic Editor: Rodrigo Picos

Received: 9 February 2025
Revised: 3 March 2025
Accepted: 4 March 2025
Published: 6 March 2025

**Citation:** Polyakov, M.V.; Sirotin, D.S. A Realistic Breast Phantom for Investigating the Features of the Microwave Radiometry Method Using Mathematical and Physical Modelling. *Technologies* **2025**, *13*, 106. https://doi.org/10.3390/technologies13030106

**Copyright:** © 2025 by the authors. Licensee MDPI, Basel, Switzerland. This article is an open access article distributed under the terms and conditions of the Creative Commons Attribution (CC BY) license (https://creativecommons.org/licenses/by/4.0/).

## 1. Introduction

Microwave radiometry is a non-invasive diagnostic method based on the measurement of natural electromagnetic radiation from human tissues in the microwave frequency range [1,2]. The use of microwave radiometry allows for the detection of temperature anomalies in the deep layers of biological tissues, which makes this method highly relevant in medicine, in particular for the early diagnosis of inflammatory processes, tumours, and other pathologies [3–5].

Accurate interpretation of measured signals is a pivotal aspect of developing the method, contingent on the physical properties of tissues and the measurement conditions. To enhance the method's informativeness, a comprehensive study of physical and mathematical models is imperative. These models delineate the processes of propagation of electromagnetic waves and their interaction with biological objects. Mathematical modelling facilitates the estimation of microwave radiation behaviour in heterogeneous tissues, accounting for temperature variations, thus enhancing the precision of diagnostics [6,7].

In recent years, microwave radiometry has witnessed significant advancements in the domain of medical diagnostics, particularly in the context of the detection and monitoring of oncological diseases, such as breast cancer [5]. A significant task in this domain pertains to the development of realistic phantoms that can accurately replicate the dielectric and

physical properties of biological tissues. The development of such phantoms is imperative for the advancement, evaluation, and substantiation of novel diagnostic instruments and algorithms.

The objective of this article is to develop a realistic breast phantom and investigate the characteristics of the microwave radiometry method through mathematical and physical modelling.

At present, there is a paucity of models that take into account the complexity of the real conditions of microwave radiometry application, which limits its wide implementation in medical practice. The necessity for the creation of complex models is determined by the requirement to enhance the precision of diagnosis and broaden the scope of application of this methodology.

The scientific novelty of the present study lies in the development and creation of a realistic breast phantom, which for the first time integrates both the anatomical and physical characteristics of biological tissue, as well as the hydrodynamics of the circulatory system. This integration allows for the accurate modelling of the processes associated with the microwave radiometry method. In contrast to existing analogues, the proposed phantom accounts for not only the dielectric properties of tissues but also their thermal characteristics, thereby ensuring a more reliable reproduction of real measurement conditions. Furthermore, the study proposes an integrated approach that combines the mathematical modelling of thermal processes with experimental verification on a physical model. This allows for the refinement of the method's parameters and an enhancement in its diagnostic accuracy. The results of the study open new opportunities for the optimisation of the microwave radiometry technique and its application in the field of medical diagnostics.

This article presents a comprehensive approach to the investigation of the features of microwave radiometry using a realistic breast phantom. Section 2 provides a comprehensive description of the functional anatomical phantom of the breast, encompassing its anatomical structure (Section 2.1.1), hardware (Section 2.1.2), and software (Section 2.1.3), along with the mathematical models of thermal processes in biological tissues (Section 2.2). Section 3 presents data from physical and mathematical modelling, the objective of which was to determine the characteristic features of the microwave radiometry method. Finally, Section 4 undertakes a thorough examination of the results obtained, along with their implications for the prospective evolution of the method within the scope of forthcoming research endeavours, summarises the key results of the study, and formulates the main conclusions.

### *1.1. Methods for Modelling Thermal Processes in Biological Tissues*

Detecting bioheat in biological tissues is a key aspect of non-invasive diagnostic methods, as temperature distribution provides essential information about metabolic activity and pathological changes. Microwave radiometry is an effective technique for assessing internal temperature without direct contact, making it valuable for early detection and monitoring of diseases such as breast cancer. Accurate physical and mathematical models are essential to improve radiometric measurements and ensure precise interpretation of temperature variations in biological tissues.

A mathematical modelling study on the influence of the menstrual cycle on breast tissue temperature demonstrated that tissue temperature was higher in the luteal phase compared to the follicular phase. These findings may have significant implications for the diagnosis and monitoring of tumour [8].

The application of infrared thermography in conjunction with bioheat transfer models for breast cancer diagnosis includes the use of dynamic techniques such as fixation thermography and rotational thermography. These approaches contribute to improved

diagnostic accuracy. Methods for post-processing thermograms and the application of artificial intelligence algorithms to analyse data [9] have also been discussed.

A general model of bioheat transfer, based on porous media theory, incorporates the thermal interaction between blood and surrounding tissues. This model is particularly well suited to modelling thermal processes in breast tissue [10]. A complex one-dimensional model of bioheat transfer that combines the hydrodynamics of arterial blood flow with heat conduction in the surrounding tissues allows a more accurate description of thermal processes in the body, including breast tissue [11]. The numerical solution of a non-linear model of bioheat transfer, incorporating energy dissipation, facilitates the estimation of tissue temperature in the presence of external heat sources, a development that may prove advantageous for the creation of thermal treatment methods.

Thermal and physiological properties of breast tissues play a crucial role in the development of diagnostic and therapeutic approaches for breast cancer. A review of the thermal and physiological properties of breast tissues, including fibroglandular, fat, and tumour tissues, indicates that data on thermal properties are limited. Consequently, approximations based on the properties of other tissues, such as muscle or fat, are frequently employed. Thus, the review [12] provides important insights into the modelling and simulation of thermal therapies, including microwave hyperthermia.

The finite difference method can be utilised to analyse bioheat transfer in breast tissue with cysts. Research has demonstrated that the dimensions and location of cysts influence the temperature field, which can be utilised for the early detection of pathologies [13,14].

Studies on the use of thermography for breast tumour detection have shown that accurate breast geometry and tumour depth are key factors for accurate temperature field and tumour detection [6]. The use of infrared thermography combined with deep learning models for breast cancer diagnosis can improve diagnostic accuracy and reduce the number of false positives [15].

A comprehensive review of methods for early detection of breast cancer using infrared thermography underscores the potential of this approach for mass screening and continuous patient monitoring [16]. Thermography and methods based on thermal modelling continue to evolve as promising tools for early detection of breast cancer. Current approaches to the use of thermography combined with deep learning show that this non-invasive and non-contact technique can detect tumours at early stages, and convolutional neural networks can automatically classify thermograms, significantly improving diagnostic accuracy [17].

Studies on the optimisation of skin cooling for enhancing thermal contrast in dynamic infrared imaging have demonstrated that cooling the breast tissue can significantly improve the detection of small and deep-seated tumours, thus making this method particularly suitable for clinical applications [18]. Physics-informed neural networks for thermal modelling in breast cancer enable the accurate reproduction of tissue thermal behaviour and can be used to develop more effective diagnostic methods relying on infrared imaging [19]. A computational thermal model for breast cancer, incorporating infrared imaging, 3D scanning, and magnetic resonance imaging data, accounts for key tumour characteristics such as size, location, and molecular subtype, thus enhancing its applicability for personalised diagnosis and treatment [20]. Breast thermography can achieve high sensitivity and specificity when strict protocols are followed. Factors such as temperature resolution, emissivity tuning, and environmental conditions should be considered to ensure the effectiveness of this technique [21].

Breast lesion screening based on infrared imaging considers the symmetry of the breast's temperature distribution and enables an objective interpretation of results, thus enhancing its applicability for large-scale screening [22]. A thermal imaging-based method for diagnosing breast tumours that analyses thermal distribution on the skin surface enables

accurate tumour diagnosis without exposure to radiation [23]. A method for estimating the size and location of a tumour that utilises skin surface temperature measurements and curve fitting enables the accurate estimation of tumour parameters at a minimal computational cost [24]. Dynamic neural networks have been shown to accurately estimate tumour parameters, including depth, size, and metabolic heat generation rate, and hold potential for clinical applications in diagnosis [25].

A modified Pennes bioheat equation that considers blood perfusion heterogeneity in tissues enables the more precise modelling of tumour thermal behaviour and may aid in optimising thermal therapies [26]. A review of current advances in infrared thermography for breast cancer detection highlights that modern infrared cameras and computational methods for heat transfer modelling have significantly improved the accuracy of thermography. However, further improvements in diagnostic capabilities require the development of new imaging protocols and the use of artificial intelligence for data analysis [27]. The potential of dynamic infrared thermography for improving breast cancer detection stems from its ability to reduce false-positive and false-negative results, thus making this technique suitable for clinical applications. The prospects of using numerical modelling and artificial intelligence to improve diagnostic accuracy are also discussed [28].

A minimally invasive thermal imaging method using nanoparticles can accurately determine the location and temperature of tumours, making it promising for cancer diagnosis and therapy [29]. The analytical solution of the Pennes equation for estimating temperature in deep tissues takes into account the different thermal properties of tissues and can be applied to model thermal processes in the body [30]. Passive microwave radiometry can measure tissue temperature at depths of up to several centimetres, making this method useful for diagnosing and monitoring diseases, such as breast cancer [1].

The use of microwave radiometry to measure brain temperature may be useful for early diagnosis and monitoring of brain injuries and strokes [31]. A review of contemporary microwave thermometry techniques for breast cancer diagnosis reveals the potential for this method to contribute to risk assessment, diagnosis, and monitoring the efficacy of treatment [32]. The challenges and prospects for the development of medical antennas for microwave radiometry are that the creation of new antenna designs can significantly improve the functionality and accuracy of medical radiothermographs [2]. The method of three-dimensional visualisation of the body's internal thermal field using multi-frequency microwave radiometry allows for more accurate localisation of hyperthermia foci, which makes it useful for breast cancer diagnosis [3].

The method of breast cancer diagnosis under investigation combines modelling and artificial intelligence algorithms, with a view to detecting small-sized tumours with high sensitivity and specificity. This makes it promising for clinical application [4]. Current methods of breast cancer diagnosis are being actively developed by integrating machine learning and neural network technologies with traditional methods such as microwave radiometry. An approach to improving the classification of microwave radiometry data using dynamic weight-independent neural networks involves optimising their topology through an evolutionary adaptation strategy of the bipopulation covariance matrix. This method has been shown to achieve a high level of accuracy in classifying patients into low- and high-risk breast cancer groups, with an F1-score of 0.933, thereby confirming the potential of microwave radiometry combined with artificial intelligence techniques for cancer diagnosis [5].

The modelling of brightness temperature in biological tissues, a fundamental component of microwave radiometry, encompasses the development of a mathematical model that considers the distribution of electromagnetic and temperature fields within the breast, acknowledging its multicomponent and heterogeneous nature. A study confirmed the

effectiveness of microwave radiometry for the diagnosis of breast diseases and provided a basis for further development of numerical models [7]. The application of cluster analysis methods to data obtained from numerical simulations of radiometric studies has shown that malignant tumours significantly affect the distribution of luminance temperature in the breast, which makes it possible to distinguish groups of patients with different tumour characteristics. This approach has the potential to be extended to model other organs and tissues [33]. The application of machine learning and neural networks to the processing of computer modelling data in medical diagnostics has also been investigated. The results of the numerical modelling of temperature fields in biological tissues were used to create training and test datasets. This approach helped to define the limits of applicability of microwave radiometry for diagnosing tumours of different sizes, which makes it promising for clinical applications [34].

Thus, current research demonstrates that the integration of machine learning, neural networks, and numerical modelling techniques with microwave radiometry offers new opportunities to improve the accuracy and efficiency of breast cancer diagnosis. These approaches not only improve data classification but also provide a deeper understanding of the effects of tumours on thermal and electromagnetic fields in tissues.

The efficiency and accuracy of diagnostic methods largely depend on a proper understanding of the physical processes underlying them and on the development of mathematical models that describe the interaction of microwave radiation with biological tissues. The application of such models allows for the improvement of the interpretation of measurement results, optimisation of equipment parameters, and development of new approaches to diagnostics.

This study aimed to develop a comprehensive approach to modelling the thermal behaviour of breast tissues, incorporating a realistic anatomical phantom and advanced numerical simulations. By integrating experimental validation and computational analysis, we sought to improve the accuracy of microwave radiometry for breast cancer diagnosis.

### *1.2. Modern Approaches to Creating Realistic Phantoms of Biological Tissues for Medical Visualisation*

The development of realistic phantoms of biological tissues is a crucial area of research in the field of medical diagnostics. Recent studies have presented the results of 3D phantoms designed for microwave monitoring and simulation of various clinical scenarios, including the detection of brain tumours, strokes, and breast cancer [35]. These phantoms have been shown to exhibit dielectric properties that closely resemble those of actual human tissues, with an error margin of 0.5–8 percent. This makes them a valuable tool for electromagnetic modelling and the testing of medical devices. A significant focus of current research efforts is on the development of tissue-equivalent phantoms for mammography. In this context, methodologies for the fabrication of such phantoms using polyvinyl alcohol, a material that exhibits atomic number and electron density characteristics analogous to those of authentic breast tissue, have been proposed. Additionally, acrylic slab phantoms simulating microcalcifications and tumours are being developed and are expected to be effective for testing mammographic systems [36,37].

The utilisation of highly accurate breast phantoms constitutes a pivotal component in the evaluation of novel microwave technologies, which offer a non-ionising and cost-effective modality for diagnostic purposes. Various techniques have been proposed for millimetre wave imaging, with the aim of creating phantoms that accurately mimic different tissue types. These techniques involve using mixtures of sunflower oil, water, and gelatin, which have been shown to reliably replicate the dielectric properties of breast tissue at frequencies up to 50 GHz [38,39]. Furthermore, phantoms based on aqueous solutions of acetonitrile have been developed, enabling tissue modelling at frequencies up to 18 GHz.

This approach is particularly relevant for the development of devices operating in body area networks [40].

Low-cost and easy-to-manufacture gel phantoms that simulate skin, muscle, blood, and fat demonstrate stable dielectric properties and are widely employed for testing wearable medical devices. Moreover, flexible and durable tissue-mimicking phantoms made from urethane mixtures containing graphite and carbon black have been developed to replicate the mechanical properties of soft tissues, such as skin [41,42].

Modern 3D printing technologies are extensively employed to create anatomical models for surgical planning and training. Various 3D printing techniques, including stereolithography and selective laser sintering, have been evaluated in terms of their suitability for the production of complex anatomical phantoms [43].

The development of phantoms also extends to magnetic resonance imaging (MRI) and ultrasound diagnostics [44]. Specifically, a breast phantom with interchangeable blocks simulating fibroglandular and adipose tissue has been developed, allowing for the quantification of relaxation parameters as well as the apparent diffusion coefficient [45]. Silicone phantoms have been proposed for diagnostic applications using Digital Imaging Elasto-Tomography which relies on the mechanical properties of tissues. The use of silicone phantoms facilitates the analysis of hysteresis loops and the detection of rigid tumour-mimicking inclusions, thereby demonstrating the effectiveness of this methodology for the early diagnosis of diseases [46].

Physical breast phantoms, constructed using computed tomography data and 3D-printing technologies, are used to optimise X-ray imaging techniques. The dielectric properties of the materials used in the fabrication of such phantoms have been investigated, with particular attention to their stability over time and their response to temperature variations. This is of critical importance in ensuring the accuracy of measurements [47–49]. A recent review highlighted the essential role of anthropomorphic breast phantoms in the advancement and refinement of imaging techniques. Advances in 3D-printing technologies have enabled the creation of highly realistic models utilised for the evaluation of diagnostic systems [50]. Furthermore, new techniques have been developed to create three-dimensional anthropomorphic phantoms, which are utilised to assess the quality of imaging in two-dimensional and three-dimensional systems [51,52].

The development of digital phantoms based on real patient data expands the possibilities in the field of X-ray diagnostics. These phantoms are used to optimise imaging techniques, including digital tomosynthesis and specialised contrast-enhanced breast imaging [53]. Furthermore, phantoms have been developed for testing elastography systems, featuring stable mechanical and acoustic properties, making them a valuable tool in diagnosis [54].

The creation of anatomically realistic numerical breast phantoms based on MRI images allows for the accurate replication of tissue dielectric properties and the modelling of microwave interactions. This contributes to the advancement of diagnostic and treatment methods [55]. Inhomogeneous phantoms simulating various tissue types (skin, adipose and glandular tissue, tumours) were utilised in microwave imaging experiments. This facilitated the investigation of the impact of inhomogeneity on image quality and the development of a novel algorithm for enhanced imaging [56,57].

Furthermore, realistic breast phantoms have been developed for the evaluation, testing, and calibration of MRI systems. In the field of microwave diagnostics, phantoms composed of household chemicals with stable dielectric characteristics have been proposed, making them a promising tool for evaluating novel cancer diagnostic methods [45,58]. Empirically generated three-dimensional computational breast phantoms have the capacity to simulate different imaging scenarios and optimise diagnostic techniques [59,60]. Physical

anthropomorphic phantoms for X-ray diagnostics, fabricated using inkjet printing, exhibit a high degree of realism and are used in digital mammography and tomosynthesis [61]. A specialised set of tumour phantoms made of polyurethane rubber with graphite and carbon powder added to reproduce different levels of malignancy has also been developed. These phantoms are actively used to test new diagnostic systems [62].

A multi-purpose breast phantom made with 3D-printing technology was designed to test various imaging modalities including mammography, contrast tomography, and MRI. It also served as a quality control tool for diagnostic systems, improving their reliability and accuracy [63].

Modern developments in the field of creating biological tissue phantoms significantly expand the possibilities of testing and improving diagnostic technologies. Figure 1 presents a structural diagram of modern approaches to creating realistic biological tissue phantoms for medical imaging. Each of these approaches encompasses specific technologies and materials used for the imitation of biological tissues. In particular, microwave phantoms are created on the basis of mixtures of sunflower oil, water, and gelatin, enabling the reliable reproduction of tissue dielectric properties. In mammography, anthropomorphic phantoms made of polymeric materials imitating fibroglandular and fat tissues are used. For ultrasound and elastographic studies, models reproducing the mechanical properties of biological tissues are being developed. Modern 3D-printing technologies, such as stereolithography and laser sintering, make it possible to create complex anatomical phantoms used in surgical planning and testing of diagnostic systems.

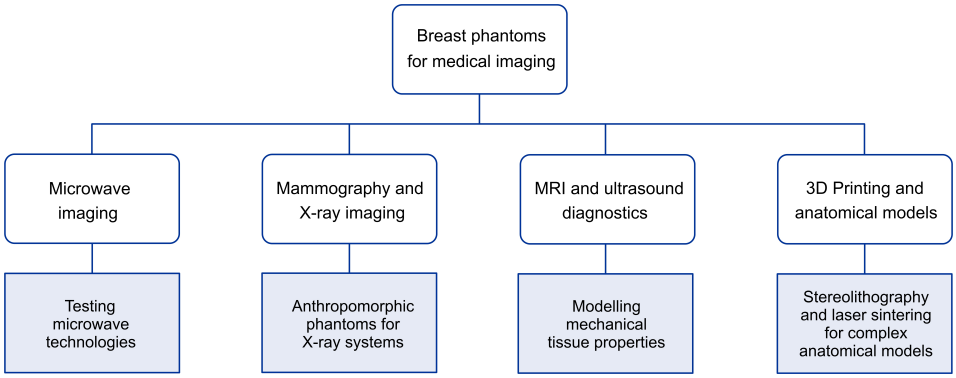



**Figure 1.** Structural diagram of modern approaches to the development of realistic phantoms of biological tissues for medical imaging.

An important area of research focusses on improving the stability of materials, improving the realism of modelled tissues, and adapting phantoms for specific clinical applications. Future research should be directed towards developing more complex and multi-component phantoms capable of simulating anatomical and physiological features of human tissues as accurately as possible.

## 2. Materials and Methods

### *2.1. Development of a Functional Anatomical Breast Phantom for Physical Modelling*

#### 2.1.1. Anatomical Structure of the Breast Phantom

The breast is a complex anatomical organ composed of skin, glandular and fat tissues, vasculature, and connective tissue (Figure 2). The nipple, surrounded by the areola, contains milk ducts that open at the surface. Fat tissue, distributed among glandular structures, provides cushioning and influences the breast shape. The glandular tissue consists of lobes connected to milk ducts, which merge into larger sinuses before reaching the surface. A well-developed vascular network, including branches of the internal thoracic, lateral thoracic, and intercostal arteries, ensures tissue nutrition and blood drainage [64].

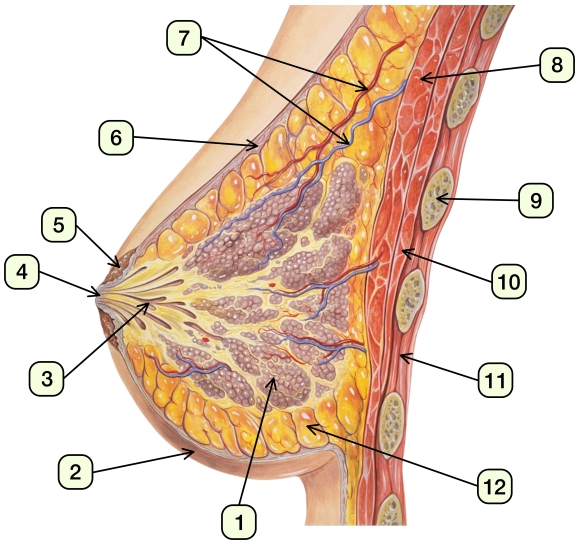



**Figure 2.** Scheme of the internal structure of the breast. In the scheme: 1—the milk lobe; 2—the skin; 3—the milky sinus; 4—the nipple; 5—the areola; 6—the subcutaneous fat tissue; 7—bloodstreams; 8—the large pectoral muscle; 9—the rib cage; 10—the small pectoral muscle; 11—intercostal muscles; 12—the fat tissue. (The basis of medical illustration: Patrick J. Lynch, medical illustrator; C. Carl Jaffe.)

The size and shape of the breast can vary, as can its location on the chest. There are different shapes of breast glands: disc-shaped, cup-shaped, hemispherical, conical, elongated.

The main morphotopometric characteristics for the described breast forms are also given. Summarising, the Table 1 presents the average values for all shapes after generalisation.

**Table 1.** Morphotopometric characteristics for different breast shapes.

| Number | Parameter | Size, cm. |
|---|---|---|
| 1 | Longitudinal diameter of the base of the breast | 7.7–11.7 |
| 2 | The circumference of the base of the breast | 34.3–41 |
| 3 | Breast height | 7.5–15.8 |
| 4 | Diameter of the areola | 2.8–7.1 |
| 5 | Nipple diameter | 0.96–1.4 |
| 6 | Nipple height | 0.29–0.5 |

The physical characteristics of the biological components were obtained from [65–70] and averaged for the breast phantom. The study measured the basic physical properties of breast phantom components, including skin, fat, glandular, and connective tissues, as well as blood flow and tumour tissue (Table 2). The measurements covered key parameters such as density, thermal conductivity, specific heat capacity, electrical conductivity and dielectric constant. A total of 14 independent measurements were made for each type of fabric to determine the mean values and the range of variation in the physical characteristics.

**Table 2.** Physical properties of biological tissues used for physical modelling

| | $\rho$ (kg/m$^3$) | $k$ (W/m·K) | $c$ (J/kg·K) | $\sigma$ (S/m) | $\varepsilon$ |
|---|---|---|---|---|---|
| Skin | 1192 | 0.46 | 3516 | 1.6 | 42 |
| Fat | 913 | 0.21 | 2494 | 0.04 | 5.2 |
| Bloodstream | 1051 | 0.52 | 3606 | 1.08 | 68 |
| Gland | 1054 | 0.48 | 3412 | 0.56 | 11 |
| Tumour | 1052 | 0.56 | 3686 | 1.21 | 48 |

Silicone is commonly used for biological tissue modelling, including skin [35,71]. The breast phantom was designed based on fundamental anatomical dimensions. The skin layer was formed as a semi-spherical shell using a mould pre-treated with a "Bc-M" release lubricant to prevent adhesion. The silicone compound was then poured in, and an air layer with controlled pressure was introduced to adjust the thickness [46,71].

After 12 h, the cured layer was removed from the mould. A nipple model was created using a similar technique, with an ethyl vinyl acetate rod heated, shaped, and solidified as a structural base. The final result is shown in Figure 3.

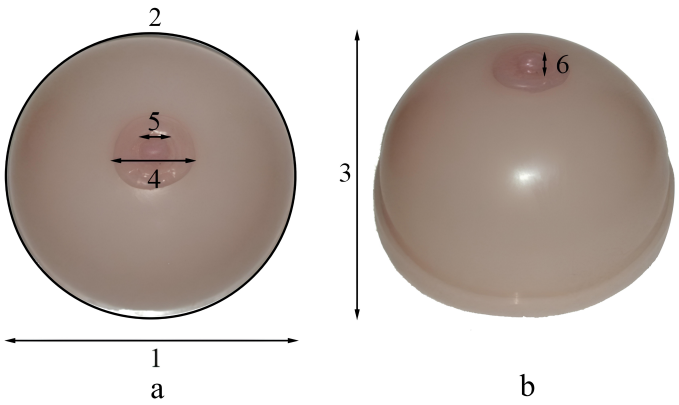



**Figure 3.** A silicone mock-up of the breast surface: top view (**a**) and frontal view (**b**).

The top and frontal projections are presented, with consideration given to the morpho-topometric characteristic number. The dimensions of each structural unit of the silicone breast model are indicated in the following.

1. Longitudinal diameter of the base of the breast—10.7 cm;
2. The circumference of the base of the breast—35.2 cm;
3. Breast height—7.8 cm;
4. Diameter of the areola—2.9 cm;
5. Nipple diameter—1 cm;
6. Nipple height—0.4 cm.

The sizes were selected to fall within the range in Table 1.

The mammary lobes, varying in number from 15 to 20, are structural units interconnected by connective tissue septa [72]. Each lobe contains a branched network of milk ducts that converge radially and open at the nipple. In the phantom, silicone tubes (3 mm internal diameter) reinforced with ethylene vinyl acetate seals were used to model the lobes. The number of lobes could be adjusted according to the experimental scenario. Each lobe was surrounded by fatty and connective tissues, ensuring anatomical accuracy (see Figure 2).

The blood supply of the breast was modelled as a network of silicone tubes with a diameter of 2 mm, allowing the use of different fluids as fillers, depending on the study. For example, a mixture of 80 percent propylene glycol and 20 percent physiological solution was employed to replicate the dielectric properties of blood tissue [73], while a water–starch solution was used to simulate blood density.

Fat tissue was modelled by considering its density and dielectric properties [35]. High-concentration gelatin has been used in studies of heating efficiency, while agar–physiological solution mixtures have been used to simulate fat tissue in other studies [73,74]. In this study, a gelatin–physiological solution mixture was used as the fat tissue model.

2.1.2. Hardware Platform for Controlling an Anatomical Breast Phantom

The hardware module of the experimental stand is a crucial component designed to ensure the safe and efficient operation of the system. It consists of several electronic components enclosed in a protective casing, which protects them from exposure to the liquids used in the simulation process. The module integrates heating elements, circulation systems, temperature sensors, and a control unit, all of which work together to regulate and monitor the thermal conditions within the phantom. Furthermore, a schematic diagram is provided to illustrate the connections and relationships between the electronic components. This section outlines the design, functionality, and integration of these elements, highlighting their significance in the experimental setup.

The hardware module constitutes a system comprising various electronic components, which are housed in a protective enclosure. The primary function of the enclosure is to prevent the exposure of electronic components to liquid during physical simulations. To provide additional protection, the liquid containers are located at a safe distance from the main electronic components.

Figure 4 shows photographs of the experimental stand hardware module enclosure from different angles, with the main dimensions indicated. In the profile projection, it is possible to distinguish five functional areas designed to accommodate electronic components. The housing is made of plastic with metal elements, which ensures its durability and resistance to external influences.

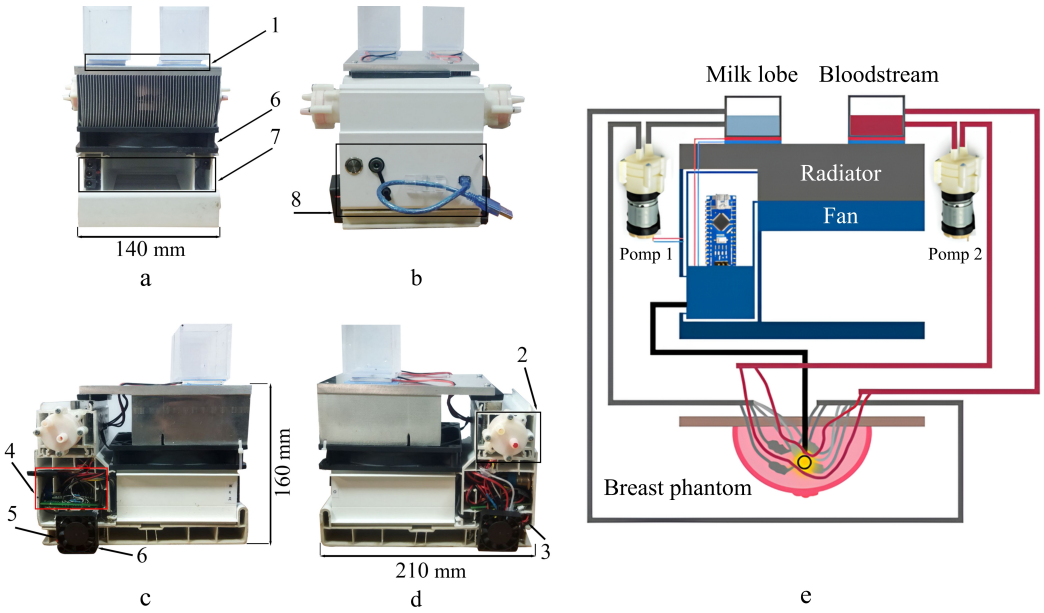



**Figure 4.** Anatomical breast phantom control device: frontal projection (front view) (**a**); frontal projection (back view) (**b**); profile projection (left view) (**c**); profile projection (right view) (**d**); diagram showing the working principle of the anatomical breast phantom control device (**e**).

Area 1 of the enclosure (Figure 4a) contains the main heating modules of the system, consisting of Peltier thermoelectric elements TEC1-12706. Their operation is controlled by an IRF520 field-effect transistor, which is located in the part of the housing marked with number 5 in Figure 4c. The main characteristics of this electronic component are given below:

- Operating temperature range: −50 to +80 °C;
- Rated DC voltage: 12 V;
- Cooling capacity: 58–65 W.

Considering the energy requirements of the system, a 120 W power supply unit (12 V, 10 A) is used to power the experimental stand, thereby ensuring the required power reserve. The main function of the Peltier element in this design is to heat the entire bottom surface of the liquid container. To increase the efficiency of operation and prevent overheating of the element, a radiator on the opposite side is used, which allows for the creation of a significant temperature gradient.

The fluid is circulated by a pump designed to run continuously for four hours. It is located in area 2 of the housing in Figure 4d.

The device is designed with ventilation openings located in the side and bottom panels of the case to ensure natural air circulation. The fans, designated by number 6 in Figure 4c, start immediately after power is supplied to pre-cool the heatsink, which helps ensure the efficient operation of the Peltier element and the stable functioning of the system. In addition, two fans are installed to cool the MOSFET transistor module and remove warm air from the main fan.

The diagnostic modules of the experimental stand include the DS18B20 temperature sensor and NTC thermistors. The contacts for their connection are marked in Figure 4a, in area 7. In the same area, on the front view, there is a connector to connect the heating element that simulates tumour development.

Figure 4c shows Area 4, which contains the Arduino Nano board, the electromagnetic relay for controlling the pump, and the 12 V power supply board. Figure 4b shows Area 8, which includes the main elements of the user interface: the device power button, the connector for the power supply, and the USB 2.0 port for communication with the Arduino Nano. Figure 4e presents a diagram showing the working principle of the anatomical breast phantom control device.

The schematic diagram of the developed hardware module is shown in Figure 5. It demonstrates the connection methods and the designation of the contacts of the electronic components used, without considering their spatial arrangement. The sensors and power elements are controlled by the Arduino Nano microcontroller, which coordinates their operation and facilitates interaction between the system modules.

The main characteristics of the Arduino Nano board used in this system are as follows:

- Microcontroller: ATmega328;
- Operating voltage (logic level): 5 V;
- DC current through I/O: 40 mAh from one pin and 500 mAh from all pins;
- Digital I/O: 14 pieces (6 of which can be used as pulse-width modulation outputs);
- Analogue inputs: 8 pieces.

We used this board due to its compact size (length is 43 mm, width is 19 mm) and sufficient performance to control the electronic components of an anatomical experimental stand.

The developed system uses three analogue and six digital pins of the microcontroller. A 47 Ω resistor is used as the heating element simulating a tumour. Its choice is due to its compact size (about 7 mm) and high heat transfer efficiency due to its large contact area with the ethylene vinyl acetate shell. Since the Arduino Nano's output current is limited, a KT815B NPN transistor is used to control the heating element, which serves as a switch. As a result, the heating element is powered directly from an external power supply, which avoids overloading the microcontroller and ensures stable operation of the system.

Data exchange between the computer and the Arduino Nano board for controlling the anatomical experimental stand is carried out via the USB serial interface, which is used to connect peripheral devices. Communication is organised via a USB-UART bridge, which enables communication through a universal asynchronous receiver-transmitter. Once the device is connected, the computer recognises the Arduino board as a device attached to the communication port.

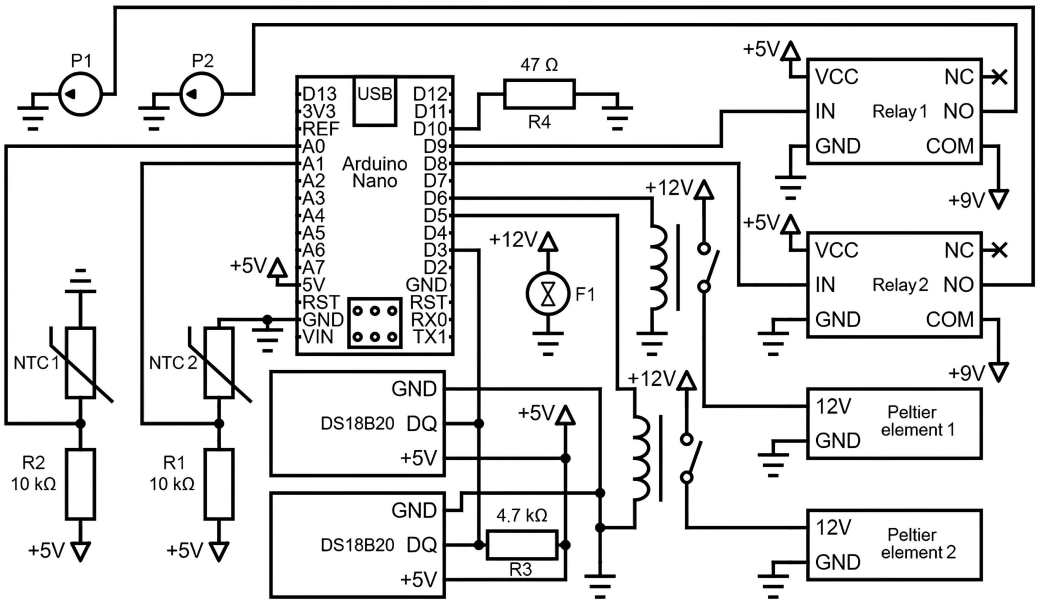



**Figure 5.** Schematic diagram of connection of the electronic components of the anatomical breast phantom control device.

The DS18B20 sensor (manufactured by Analog Devices Inc., Wilmington, MA, USA) is used to measure temperature using the OneWire protocol. This protocol allows communication with multiple devices over a single digital line, simplifying wiring.

The heating element temperature is controlled by pulse-width modulation, where the applied voltage is varied by modulating the pulse width, allowing flexible control of the heating power.

#### 2.1.3. Software Part for Controlling a Functional Anatomical Breast Phantom

The software module of the anatomical experimental stand is responsible for the automated control and monitoring of all active system components. Implemented on the Arduino platform, it ensures the precise regulation of heating elements, fluid circulation, temperature sensors, and real-time data exchange with a computer. The software consists of several functional modules, including system initialisation, data acquisition, heating and cooling management, and communication via a USB-UART interface. By integrating these components, the software provides efficient control over the experimental process, which allows real-time adjustments and data recording to ensure accurate and reproducible results.

The software for the anatomical experimental setup was implemented on the Arduino platform, which provided control over all active components of the system, including the heating element, fluid circulation system, temperature sensors, and the interface with the computer.

The main functions of the software module included the following:

- Collect and process data from temperature sensors to control and regulate heating;
- Control of the tumour-simulating heating element using pulse-width modulation for precise temperature control;
- Operation of a cooling system that includes fans to maintain the thermal behaviour of the Peltier elements;
- Control of fluid circulation by means of an electromagnetic relay and a pump that ensures constant fluid movement inside the anatomical breast phantom;
- Data exchange with the computer via a USB-UART interface, which allows one to transfer the measured parameters and receive control commands.

The programme was loaded on the Arduino Nano (manufactured by Arduino S.r.l., Monza, Italy) board and written in C++ language using standard Arduino IDE libraries. The software consisted of the following modules: system initialisation module, data reading module, heating element control module, circulation system control module, cooling system control module, and data exchange module with the computer.

The system initialisation module allows the user to define the digital and analogue pins to be used. It also allows the user to set up serial communication with a computer and to set initial heating and cooling parameters. The sensor readout module allows the user to query the DS18B20 for temperature via OneWire and read analogue values from the NTC thermistors and convert them to temperature. The heater control module allows the user to use a PWM signal to regulate the voltage supply to the heating resistor. This module also provides the user with the ability to control a transistor to turn the heating on/off. The circulation system control module is responsible for controlling the pump via an electromagnetic relay and maintaining the optimum fluid flow rate. The cooling system control module automatically starts the fans when the experimental stand is powered on and cools the Peltier element's radiator to maintain the temperature gradient in the system. The PC communication module sends the current system parameters (temperature, heating, and circulation status) via UART and receives commands from the user, including temperature adjustments and switching components on/off.

Figure 6 shows the program flow diagram, which provides a step-by-step description of the operation of the anatomical breast phantom control programme. During the operation of the program, first, the port for connecting the device is selected, and then the device is checked to determine if it is properly connected. Then, the user selects a directory to save the files, specifies a name for the experiment file, and starts the experiment. An important part of the programme is to wait for the required temperature to be reached in different parts of the anatomical phantom such as fat tissue, bloodstreams, and mammary lobes. Once the temperature in these areas has stabilised within an acceptable range, the program continues with data entry such as the temperature of the bloodstream, milk lobes, and tumour. The phantom temperature is then measured, and these values are saved to a file. If this is not the final experiment, the program returns to the initial stage; otherwise, it resets all values and ends the experiment. The diagram reflects the sequence of actions, including temperature control, data saving and experiment termination, which demonstrates the structure of interaction between the different components of the programme.

The software component provides flexibility to the system, allowing parameters to be changed in real time through the computer and controlling all physical modelling processes.

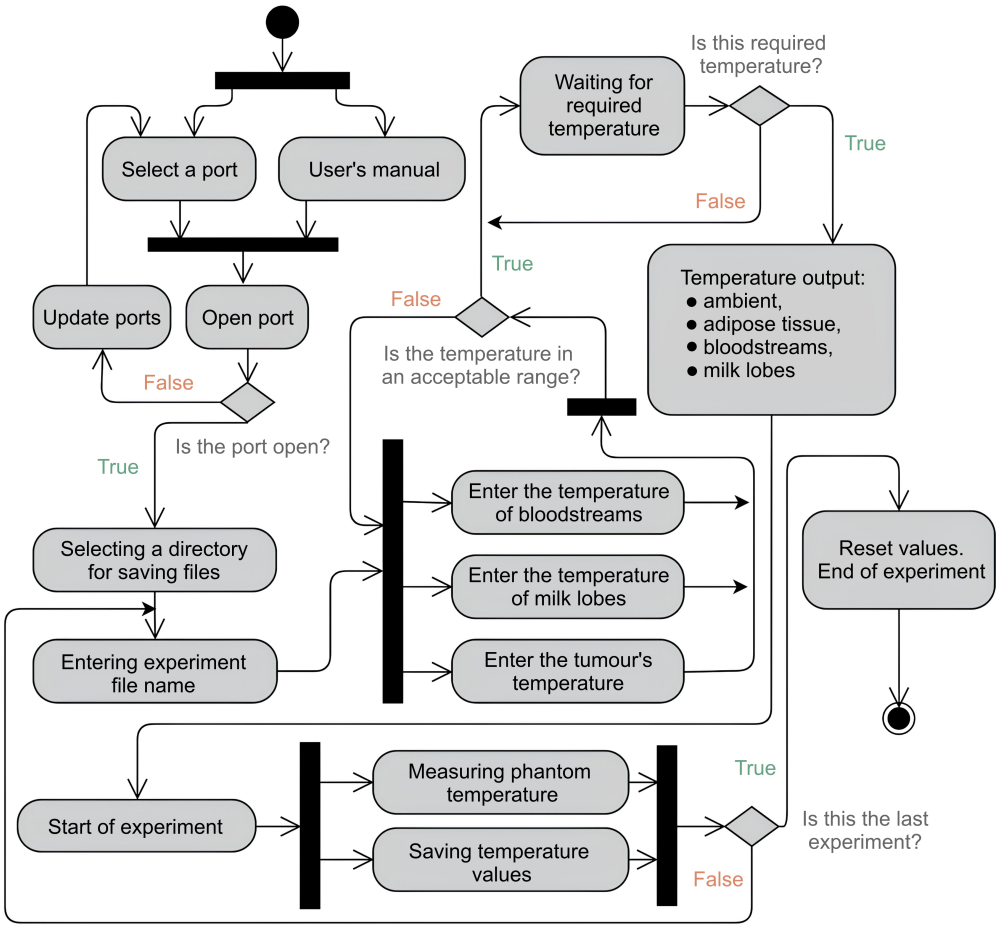



**Figure 6.** Activity diagram of the anatomical breast phantom control software.

### *2.2. Mathematical and Numerical Modelling of Thermal Processes in Biological Tissues*

To model the dynamics of thermal processes in biological tissues, we used the equation of heat transfer with consideration of sources

$$\rho(\vec{r})C(\vec{r})\frac{\partial T(\vec{r},t)}{\partial t} = \nabla\lambda(\vec{r})\nabla T + Q_{met}(\vec{r},t) + Q_{can}(\vec{r}), \quad (1)$$

where $T$ is the temperature, $\rho$ is the density, $C$ is the specific heat capacity, $\lambda$ is the heat transfer coefficient, $\vec{r} = \{x, y, z\}$, $\nabla$ is the nabla operator. We distinguished the following sources of heat-source power density due to metabolic processes, produced by the metabolic processes in tissues ($Q_{met}$) and the cancerous tumours ($Q_{can}$) The important distinguishing features of the model were the consideration of spatial heterogeneity of all the main physical parameters and the consideration of the circulatory system as a self-consistent part of the model geometry. At the same time, the bloodstream temperature for the model was taken as $T_{bl} = 37\ ^{\circ}\mathrm{C}$.

At the boundary between the biological tissue and the environment, we set the condition of continuity of energy flow

$$\lambda(\vec{r})\vec{n}\nabla T(\vec{r},t) = h(T_{air} - T(x,y,z,t)), \quad (2)$$

where $\vec{n}$ is the vector of normal to the interface "biotissue–environment", $h$ is the heat transfer coefficient ($\mathrm{W/m^2 \cdot ^{\circ}C}$), $T_{air}$ is the ambient temperature. The ambient temperature was set to the same value as in the physical experiment.

The contact between the breast tissue and the underlying muscle layer was incorporated into the model, as described by the appropriate boundary conditions. The temperature $T$ = 37 °C was set at the interface between the breast tissue and the underlying muscle layer.

A numerical analysis was performed using the finite element method. For the verification of the model, data from physical experiments on the created breast phantom were used, allowing for the comparison of theoretical and experimental results.

The finite element method is widely used for the numerical solution of the heat conduction equation in biological tissues and allows for the consideration of complex geometry, anisotropic properties, and the presence of internal heat sources. A biological tissue is discretised into a finite number of small subareas called finite elements. We used tetrahedra as finite elements. Within each element, the temperature is represented as an interpolation function based on the temperature values at the mesh nodes. To obtain a numerical solution, we used the Galerkin method, which involves multiplying the equation by the basis functions $\phi_i$ and integrating over the entire volume of the computational domain $V$:

$$\int_V \rho C \frac{\partial T}{\partial t} \phi_i dV + \int_V \lambda \nabla T \cdot \nabla \phi_i dV = \int_V (Q_{met} + Q_{can}) \phi_i dV. \quad (3)$$

Applying integration by parts to the diffusion term and replacing continuous temperature fields by their finite element representations, the equation is reduced to a system of algebraic equations. After discretisation of the equation, the obtained system is written in matrix form:

$$[C] \frac{dT}{dt} + [\lambda] T = Q, \quad (4)$$

where $[C]$ is the heat capacity matrix, $[\lambda]$ is the stiffness matrix describing heat conduction processes, and $Q$ is the right-hand side vector including heat sources.

Then, the obtained system of equations was solved numerically using the method of conjugate gradients. To solve the problem of heat conduction in biological tissues using the finite element method, specialised software was developed in C++ using parallel computing on graphics processors (GPU NVIDIA RTX 4000 (manufactured by PNY Technologies Inc., Parsippany, NJ, USA)) with the help of CUDA technology.

The programme was a computational module that included the following main components:

- Discretisation module for creating a finite element mesh for the 3D model;
- Module for assembling a system of equations to form global matrices;
- Numerical solution module for using parallel algorithms to solve a sparse system of linear equations.

To discretise the model, the open-source grid generator Netgen (GNU LGPL licence) was used to create a three-dimensional grid of tetrahedra. Each element contained nodes that stored temperature values. The system of equations was represented as a sparse matrix using the CSR (Compressed Sparse Row) format, which is optimised for GPU operation. CUDA was used to update the temperature at the grid nodes in parallel. In each GPU thread, a new temperature value was calculated for one node.

## 3. Results

### *3.1. Results of Physical Modelling of Thermal Processes in the Breast Phantom*

The temperature measurement using radio-microwave thermometry was carried out according to the setup shown in Figure 7a. In the course of measurements, the antenna-applicator of the radiometer was moved uniformly over the surface of the breast, and each

temperature value was recorded for at least five seconds. The ambient temperature during the experiment was $T_{air}$ = 26.5 °C.

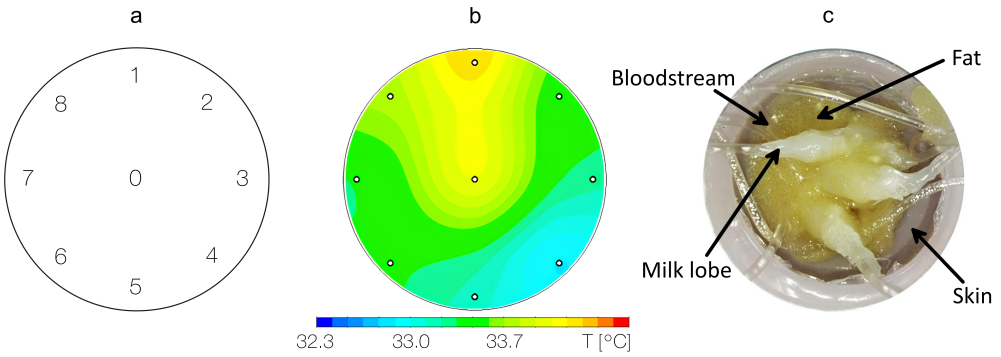



**Figure 7.** Schematic of breast temperature measurement by microwave radiometry (**a**); temperature distribution inside the anatomical breast phantom in the radio-microwave range (**b**); internal structure of the anatomical breast phantom (**c**).

The experiments aimed to analyse temperature data obtained with the antenna-applicator of the RTM-01-RES radiometer (manufactured by RES Ltd., Moscow, Russia) and from temperature sensors placed in the bloodstream, milk lobes, and fat tissue.

The first stage of the experiment involved determining the temperature differences in an area without local heat sources and in the absence of a tumour within the phantom. This study was necessary for the subsequent analysis of the thermal characteristics of the model. The measurement results are presented as a heat map (see Figure 7b) and a photograph of the physical structure of the investigated breast (see Figure 7c).

The lowest temperature values were recorded in areas "3"–"5", with the temperature difference between points "0" and "4" being 1.2 °C. This is due to the smaller number of mammary lobes in that area of the layout, their displacement to the upper layers, and the absence of bloodstream.

The second experiment aimed to measure the temperature of the skin surface using the antenna adapter of the RTM-01-RES radiometer (Figure 8a) and a contact infrared sensor (Figure 8b). During the experiment, the heat sources in the form of bloodstream were concentrated in the region of "0"–"2" points.

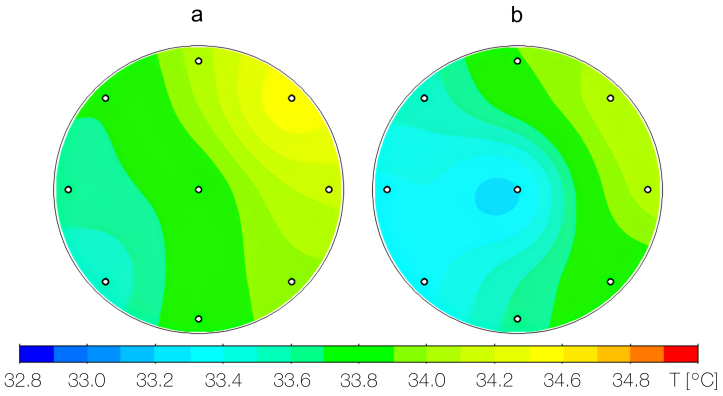



**Figure 8.** Temperature distribution of the anatomical breast phantom: internal temperature in the microwave range (**a**); skin temperature in the infrared range (**b**).

The data analysis showed that moving the heat source relative to the conditions in the first experiment (see Figure 7c) resulted in a corresponding change in radiometer readings, confirming the accuracy of temperature modelling in the phantom. On average, the temperature on the skin surface differed from the internal values by 0.26 °C, with a difference of 0.6 °C at point "0", likely due to the increased thickness of the silicone

layer in that area. At the same time, the internal temperature of the layout elements remained unchanged.

In the third experiment, the position of the internal temperature sensor was changed with each new measurement. Thus, the temperature in the direction plane of the applicator antenna was measured in three positions: on the skin, close to the surface of the skin layer, and inside the layout at a depth of 3 cm. The measurement results are presented in Figure 9. According to the data obtained, the temperature recorded by the antenna and the subcutaneous sensor differed from the temperature measured at higher depths by an average of 0.3 °C. This suggests that maximum measurement accuracy was achieved near the subcutaneous layer, as most of the signal was generated directly beneath the antenna. It should also be taken into account that the density and dielectric constant of the materials used can affect the overall temperature pattern.

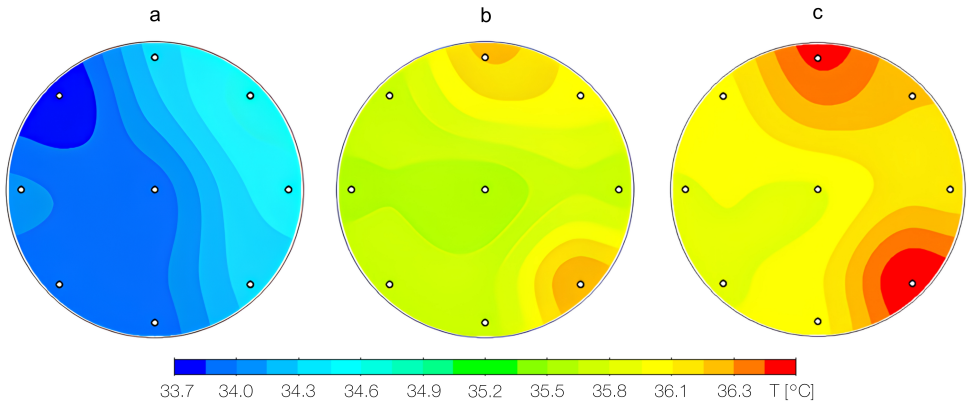



**Figure 9.** Thermodynamic temperature distribution at different depths: on the skin surface (**a**); under the skin (**b**); at a depth of 3 cm (**c**).

The final physical experiment was designed to investigate the effect of a local heat source simulating a tumour. A region with an increased temperature was added to the system that exceeded the initial values by 2 ° C. The initial temperature state of the phantom is shown in Figure 10a, with an average temperature of 34.12 °C. After placing the tumour in the region of point "3", the temperature at that point and its vicinity (points "1"–"5") increased by an average of 0.31 °C, with a local increase of 0.77 °C at point "3" relative to the mean value (Figure 10b). The tumour was located 1 cm below the skin layer.

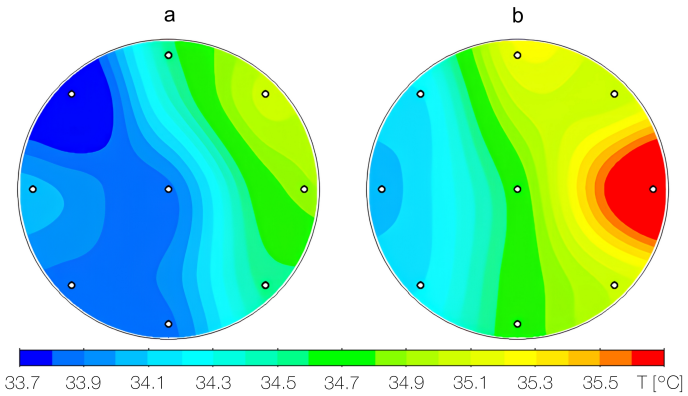



**Figure 10.** Internal temperature distribution for breast phantom without internal heat source simulating tumour (**a**); with internal heat source simulating tumour at "3" (**b**).

Therefore, the experiment demonstrated that a local temperature increase corresponding to the presence of a tumour could be detected by microwave radiometry. The largest temperature difference was observed near the heat source, which aligned with the expected physiological characteristics. The obtained results demonstrated that the developed

anatomical phantom reliably reproduced temperature gradients characteristic of pathological changes in breast tissue. This confirmed its suitability for further studies aimed at evaluating thermographic diagnostic methods. Future experiments are planned to investigate the influence of various tumour parameters, such as depth, size, and degree of thermal abnormality, on the efficiency of the measurements.

The graph in Figure 11 shows the temperature distribution for different tissue types, including skin, adipose, glandular, connective tissue, bloodstream, and tumour tissue. For each tissue, the mean temperature measured during the experiments is presented along with confidence intervals that reflect the range of possible temperature variations. The confidence intervals were constructed at a significance level of 95 percent and take into account the variability of temperature measurements associated with tissue heterogeneity and possible errors of the method. The analysis of the obtained data showed that tumour tissues demonstrated higher temperatures compared to the surrounding healthy tissues, which is in line with expectations associated with the increased metabolic activity of the tumour and altered blood supply. In contrast, adipose tissue had the lowest average temperature values, which is explained by its low thermal conductivity. The presented data confirmed the stability of the measurement technique and allowed us to quantify the variation in temperature values for different tissue types, which is important for further statistical analysis and development of diagnostic criteria.

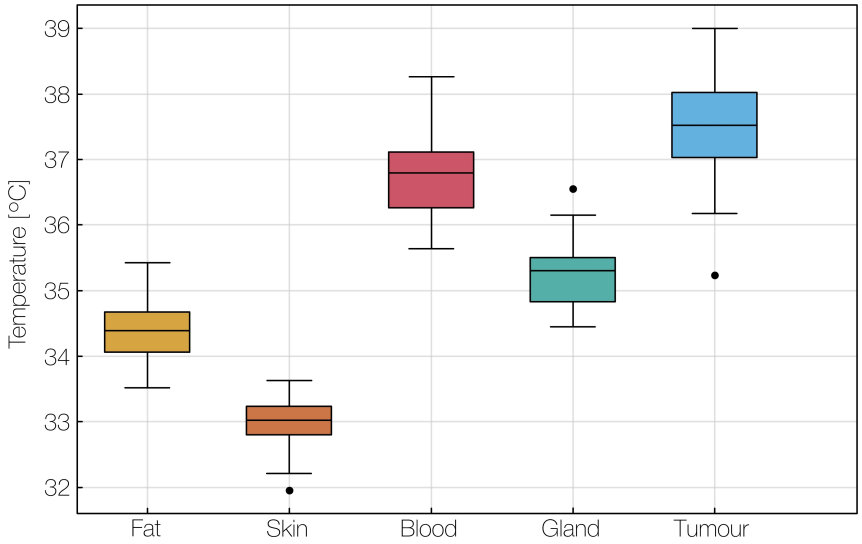



**Figure 11.** Temperature distribution for different tissue types (skin, fat tissue, glandular tissue, bloodstream, tumour tissue).

### *3.2. Results of Mathematical Modelling to Determine the Characteristic Features of the Microwave Radiometry Method*

The mathematical modelling was conducted based on the solution to the heat conduction Equation (1). A three-dimensional finite element model of the breast, incorporating a heterogeneous distribution of thermal conductivity, heat capacity, and bloodstream coefficients, was used for the calculations. The parameters of the physical experiment were identical to the numerical simulation, including external heat transfer conditions and blood circulation rate. The geometry of the model was fully consistent with that of the breast phantom structure.

The temperature distribution profiles obtained from mathematical and physical modelling were then compared to analyse the results.

A fundamental objective of the study was to ascertain temperature anomalies resulting from fluctuations in the bloodstream within biological tissues. In the course of numerical modelling, it was found that in areas with increased perfusion (simulating pathological

areas), the temperature increased by 0.8–1.2 °C compared to the surrounding normal tissue. Mathematical modelling showed that increased perfusion in certain areas led to an increase in temperature in these areas. This is explained by the increased inflow of warm blood, which maintains a temperature of about 37.0 °C, while the surrounding tissues, which have less perfusion, are cooled by heat conduction and convective heat exchange with the external environment. In a physical experiment with a breast phantom, a similar effect was confirmed using an integrated fluid circulation system simulating the bloodstream. The use of temperature sensors at different points of the phantom showed that when the fluid circulation rate increased in certain zones, a temperature increase of 0.9–1.1 °C was observed, which was in good agreement with the results of the numerical modelling.

The congruence of experimental and numerical data thus indicates that the mathematical model provides an adequate description of the processes of heat transfer in biological tissues and can be utilised to predict temperature changes in various physiological and pathological conditions.

Another important result of the modelling was the study of temperature gradients occurring in the area of pathological changes. During numerical modelling, it was found that the temperature gradient in areas with increased perfusion was significantly higher than in the surrounding normal tissue. This is due to the sharper temperature difference between the hot blood and the surrounding medium. In normal tissues, temperature changes occur smoothly, whereas in pathological areas, pronounced thermal contrasts are formed. When data from physical experiments were analysed, it was found that the temperature distribution in the phantom also exhibited enhanced temperature gradients in areas with active fluid circulation. These results were confirmed by infrared thermography as well as data from contact thermocouples placed at various points in the phantom. Experimental measurements showed that the microwave radiometry method could register deep temperature contrasts caused by changes in the bloodstream, confirming its diagnostic value for detecting thermal anomalies.

Figure 12 shows a comparison of the temperature profiles obtained by numerical modelling using the finite element method and physical experiment on a breast phantom. The graph shows the variation in temperature as a function of tissue depth (in the range of 0.5–5.0 cm). The numerical modelling data are indicated by blue markers (solid line), and the results of the physical experiment are shown by red markers (dashed line). In the surface layers (0.5–2.0 cm), the temperature remained relatively low (34.3–34.8 °C) in both numerical and physical simulations. In deeper layers (3.0–5.0 cm), a smooth increase in temperature was observed, associated with an increased influence of bloodstream and decreased heat transfer to the environment. The difference between numerical and experimental temperatures did not exceed 0.2 °C, which indicated a high accuracy of the mathematical model. The greatest discrepancy was observed at depths of 4–6 cm, which may be related to the variability in the thermophysical properties of the phantom material and peculiarities of measurements.

Table 3 presents a comparative analysis of key results from physical experiment and numerical simulation. As can be seen from the data, the model showed a high degree of agreement with the experimental measurements. The difference in temperature gradient between the subcutaneous layer and the deep region was 0.3 °C in the experiment and 0.28 °C in the simulation, corresponding to a deviation of less than 7 percent. The base temperature of the system in both cases coincided with an error of less than 0.2 percent, which confirmed the correctness of the selected heat transfer parameters. The local temperature increase in the tumour region was 0.77 °C in the experiment and 0.74 °C in the numerical simulation, demonstrating the high sensitivity of the method to thermal anomalies. The deviation for the temperature increase at a depth of 1 cm due to the presence of tumour

was 6.5 percent, which was within acceptable errors. The correlation coefficient between the experimental and modelled data was 0.98, which indicated the high accuracy of the model and its applicability for the analysis of thermal processes in biological tissues.

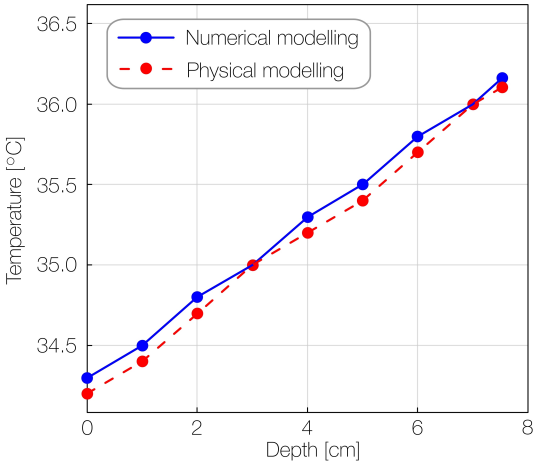



**Figure 12.** Comparison of temperature profiles obtained from numerical modelling (blue markers) and physical experiment (red markers) as a function of tissue depth.

Figure 13 is a comparative analysis of the temperature distribution obtained using three different approaches: data recorded from real patients (a, b) [4], numerical modelling (c, d), and physical models (e, f). The abscissa axis shows the luminance temperature $T_B$ in the study area, and the ordinate axis shows the number of observations for each method. The histograms demonstrate that the temperature distributions obtained by numerical and physical modelling have a high degree of agreement with clinical data, which confirms the validity of the developed models.

The microwave radiometry method was used to verify the numerical and physical modelling data. Experimental measurements showed that the method was able to register deep temperature contrasts caused by changes in bloodstream, which confirmed its diagnostic significance for detecting thermal anomalies.

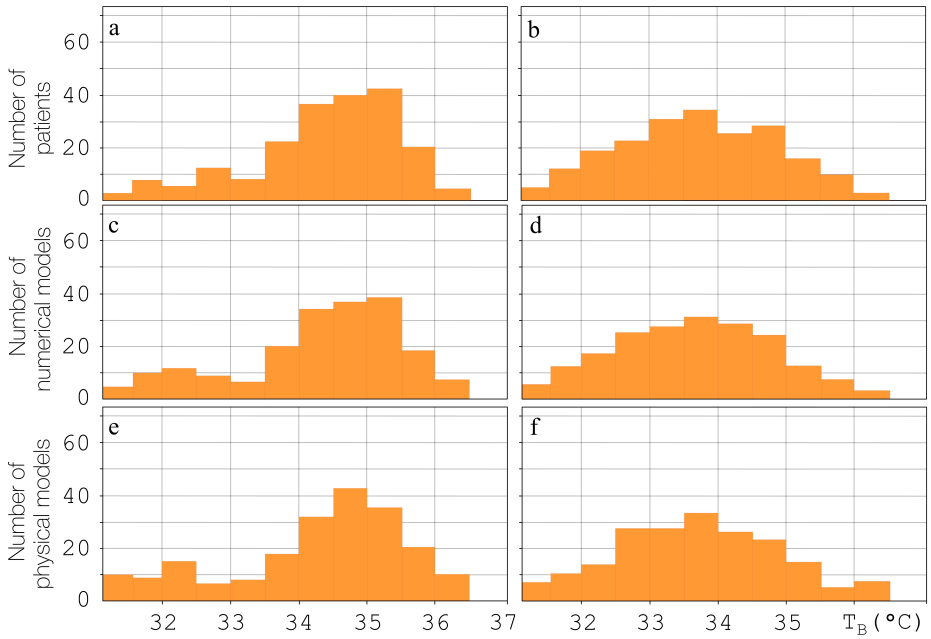



**Figure 13.** Comparison of temperature distributions at the "0" point obtained from clinical data (**a**,**b**), numerical simulations (**c**,**d**), and physical models (**e**,**f**).

**Table 3.** Comparison of key results from physical and numerical modelling.

| Parameter | Physical Experiment | Numerical Modelling | Deviation (%) |
|---|---|---|---|
| Temperature difference (subcutaneous—deep layer), °C | 0.3 | 0.28 | 6.7 |
| Baseline system temperature, °C | 34.12 | 34.05 | 0.2 |
| Local temperature increase in tumour region, °C | 0.77 | 0.74 | 3.9 |
| Temperature increase at 1 cm depth due to tumour, °C | 0.31 | 0.29 | 6.5 |
| Correlation coefficient (model vs. experiment) | — | 0.98 | — |

## 4. Discussion and Conclusions

One of the key factors that affect the accuracy of microwave radiometry is the presence of potential errors that arise from modelling and experimentation. One such source of error is the potential deterioration of phantom materials over time, especially with repeated use and exposure to external conditions such as temperature and humidity. In particular, hydrogel and polymer components that mimic biological tissues can change their dielectric and thermal properties, potentially affecting the reproducibility of measurements. An additional factor is the individual diversity of breast composition in different patients, including variations in the percentage of fat, glandular, and connective tissue. These differences can lead to variations in thermal distribution and thus affect diagnostic accuracy. In the future, additional calibration measurements and the development of adaptive correction algorithms that take into account individual anatomical features are possible to minimise these effects.

The simulation results demonstrated that pathological changes in tissue properties had a significant impact on temperature distributions, supporting the use of these data for pathology localisation, as shown in previous studies [5,15]. The proposed approach offers several advantages over existing models [36,58]. Firstly, it integrates both mathematical and physical models, allowing for a more comprehensive consideration of complex thermal interactions. Secondly, the model is specifically adapted for clinical environments, which enhances its practical applicability. These features collectively strengthen the potential of microwave radiometry for improving diagnostic capabilities. Integrating these advanced modelling techniques into microwave radiometry not only enhances its effectiveness but also paves the way for further developments, including the adaptation of models to account for individual patient characteristics [1,2,4]. Future research in this area could focus on refining these adaptive models to tailor them more closely to the unique conditions of each patient.

**Author Contributions:** Conceptualization, M.V.P.; methodology, D.S.S.; software, D.S.S.; formal analysis, D.S.S. validation, M.V.P. and D.S.S.; investigation, M.V.P.; data curation, D.S.S.; writing—original draft preparation, M.V.P.; visualization, M.V.P. and D.S.S.; supervision, M.V.P. All authors have read and agreed to the published version of the manuscript.

**Funding:** This work supported by the Russian Science Foundation (grant no. 23-71-00016, https://rscf.ru/project/23-71-00016/ (accessed on 5 March 2025). The research also relied on the shared research facilities of the HPC computing resources at Lomonosov Moscow State University.

**Data Availability Statement:** Data are contained within the article.

**Conflicts of Interest:** The authors declare no conflicts of interest.

## References

1. Goryanin, I.; Karbainov, S.; Shevelev, O.; Tarakanov, A.; Redpath, K.; Vesnin, S.; Ivanov, Y. Passive Microwave Radiometry in Biomedical Studies. *Drug Discov. Today* **2020**, *25*, 757–763. [CrossRef]
2. Sedankin, M.K.; Leushin, V.Y.; Agasieva, S.V.; Gudkov, A.G.; Vesnin, S.G.; Porokhov, I.O.; Antonenkova, A.Y. Medical Antennas for Microwave Radiothermometry of Biological Objects. *Biomed. Eng.* **2023**, *56*, 419–423. [CrossRef]

3. Sidorov, I.A.; Gudkov, A.G.; Leushin, V.Y.; Gorlacheva, E.N.; Novichikhin, E.P.; Agasieva, S.V. Measurement and 3D Visualization of the Human Internal Heat Field by Means of Microwave Radiometry. *Sensors* **2021**, *21*, 4005. [CrossRef] [PubMed]
4. Khoperskov, A.V.; Polyakov, M.V. Improving the Efficiency of Oncological Diagnosis of the Breast Based on the Combined Use of Simulation Modeling and Artificial Intelligence Algorithms. *Algorithms* **2022**, *15*, 292. [CrossRef]
5. Li, J.; Galazis, C.; Popov, L.; Ovchinnikov, L.; Kharybina, T.; Vesnin, S.; Losev, A.; Goryanin, I. Dynamic Weight Agnostic Neural Networks and Medical Microwave Radiometry (MWR) for Breast Cancer Diagnostics. *Diagnostics* **2022**, *12*, 2037. [CrossRef]
6. Mukhmetov, O.; Igali, D.; Mashekova, A.; Zhao, Y.; Ng, E.Y.K.; Fok, S.C.; Teh, S.L. Thermal Modeling for Breast Tumor Detection Using Thermography. *Int. J. Therm. Sci.* **2021**, *161*, 106712. [CrossRef]
7. Polyakov, M.; Levshinskii, V.; Khoperskov, A. Modeling of Brightness Temperature in Biological Tissue. *J. Phys. Conf. Ser.* **2019**, *1368*, 042057. [CrossRef]
8. Shrestha, S.; Gurung, D.B.; Gokul, K.C. Mathematical Modeling of Temperature Variation in Breast Tissue with and without Tumor/Cyst During Menstrual Cycle. *Math. Model. Comput.* **2021**, *8*, 192–202. [CrossRef]
9. D'Alessandro, G.; Tavakolian, P.; Sfarra, S. A Review of Techniques and Bio-Heat Transfer Models Supporting Infrared Thermal Imaging for Diagnosis of Malignancy. *Appl. Sci.* **2024**, *14*, 1603. [CrossRef]
10. Nakayama, A.; Kuwahara, F. A General Bioheat Transfer Model Based on the Theory of Porous Media. *Int. J. Heat Mass Transf.* **2008**, *51*, 3190–3199. [CrossRef]
11. Coccarelli, A.; Boileau, E.; Parthimos, D.; Nithiarasu, P. An Advanced Computational Bioheat Transfer Model for a Human Body with an Embedded Systemic Circulation. *Biomech. Model. Mechanobiol.* **2016**, *15*, 1173–1190. [CrossRef]
12. Camilleri, J.S.; Farrugia, L.; Curto, S.; Rodrigues, D.B.; Farina, L.; Caruana Dingli, G.; Sammut, C.V. Review of Thermal and Physiological Properties of Human Breast Tissue. *Sensors* **2022**, *22*, 3894. [CrossRef] [PubMed]
13. Abdalla, A.; Abbas, I.; Sapoor, H. The Numerical Estimation of Temperature in Living Tissue with Energy Dissipation Using Nonlinear Bioheat Model. *Indian J. Phys.* **2022**, *96*, 3477–3483. [CrossRef]
14. Patil, H.M.; Maniyeri, R. Finite Difference Method Based Analysis of Bio-Heat Transfer in Human Breast Cyst. *Therm. Sci. Eng. Prog.* **2019**, *10*, 42–47. [CrossRef]
15. Mambou, S.J.; Maresova, P.; Krejcar, O.; Selamat, A.; Kuca, K. Breast Cancer Detection Using Infrared Thermal Imaging and a Deep Learning Model. *Sensors* **2018**, *18*, 2799. [CrossRef] [PubMed]
16. Mashekova, A.; Zhao, Y.; Ng, E.Y.; Zarikas, V.; Fok, S.C.; Mukhmetov, O. Early Detection of the Breast Cancer Using Infrared Technology–A Comprehensive Review. *Therm. Sci. Eng. Prog.* **2022**, *27*, 101142. [CrossRef]
17. Roslidar, R.; Rahman, A.; Muharar, R.; Syahputra, M.R.; Arnia, F.; Syukri, M.; Munadi, K. A Review on Recent Progress in Thermal Imaging and Deep Learning Approaches for Breast Cancer Detection. *IEEE Access* **2020**, *8*, 116176–116194. [CrossRef]
18. Zhou, Y.; Herman, C. Optimization of Skin Cooling by Computational Modeling for Early Thermographic Detection of Breast Cancer. *Int. J. Heat Mass Transf.* **2018**, *126*, 864–876. [CrossRef]
19. Perez-Raya, I.; Kandlikar, S.G. Thermal Modeling of Patient-Specific Breast Cancer with Physics-Based Artificial Intelligence. *ASME J. Heat Mass Transf.* **2023**, *145*, 031201. [CrossRef]
20. Lozano, A.; Hayes, J.C.; Compton, L.M.; Azarnoosh, J.; Hassanipour, F. Determining the Thermal Characteristics of Breast Cancer Based on High-Resolution Infrared Imaging, 3D Breast Scans, and Magnetic Resonance Imaging. *Sci. Rep.* **2020**, *10*, 10105. [CrossRef]
21. Ng, E.K. A Review of Thermography as Promising Non-Invasive Detection Modality for Breast Tumor. *Int. J. Therm. Sci.* **2009**, *48*, 849–859. [CrossRef]
22. Morais, K.C.C.; Vargas, J.V.C.; Reisemberger, G.G.; Freitas, F.N.P.; Oliari, S.H.; Brioschi, M.L.; Neto, C.D. An Infrared Image Based Methodology for Breast Lesions Screening. *Infrared Phys. Technol.* **2016**, *76*, 710–721. [CrossRef]
23. Shi, G.L.; Han, F.; Liang, C.W.; Wang, L.; Li, K.Y. A Novel Method of Thermal Tomography Tumor Diagnosis and Its Clinical Practice. *Appl. Therm. Eng.* **2014**, *73*, 408–415. [CrossRef]
24. Das, K.; Mishra, S.C. Non-Invasive Estimation of Size and Location of a Tumor in a Human Breast Using a Curve Fitting Technique. *Int. Commun. Heat Mass Transf.* **2014**, *56*, 63–70. [CrossRef]
25. Saniei, E.; Setayeshi, S.; Akbari, M.E.; Navid, M. Parameter Estimation of Breast Tumour Using Dynamic Neural Network from Thermal Pattern. *J. Adv. Res.* **2016**, *7*, 1045–1055. [CrossRef] [PubMed]
26. Singh, M. Modified Pennes Bioheat Equation with Heterogeneous Blood Perfusion: A Newer Perspective. *Int. J. Heat Mass Transf.* **2024**, *218*, 124698. [CrossRef]
27. Kandlikar, S.G.; Perez-Raya, I.; Raghupathi, P.A.; Gonzalez-Hernandez, J.L.; Dabydeen, D.; Medeiros, L.; Phatak, P. Infrared Imaging Technology for Breast Cancer Detection–Current Status, Protocols and New Directions. *Int. J. Heat Mass Transf.* **2017**, *108*, 2303–2320. [CrossRef]
28. Gonzalez-Hernandez, J.L.; Recinella, A.N.; Kandlikar, S.G.; Dabydeen, D.; Medeiros, L.; Phatak, P. Technology, Application and Potential of Dynamic Breast Thermography for the Detection of Breast Cancer. *Int. J. Heat Mass Transf.* **2019**, *131*, 558–573. [CrossRef]

29. Gescheit, I.M.; Dayan, A.; Ben-David, M.; Gannot, I. Minimal-Invasive Thermal Imaging of a Malignant Tumor: A Simple Model and Algorithm. *Med. Phys.* **2010**, *37*, 211–216. [CrossRef]
30. Akpolile, A.; Mokobia, E.; Ikubor, J. Analytical Approach to the Penne's Bioheat Equation for the Evaluation of Temperature for Deep Seated Tissues. *Adv. Math. Sci. J.* **2021**, *10*, 2957–2976. [CrossRef]
31. Shevelev, O.; Petrova, M.; Smolensky, A.; Osmonov, B.; Toimatov, S.; Kharybina, T.; Goryanin, I. Using Medical Microwave Radiometry for Brain Temperature Measurements. *Drug Discov. Today* **2022**, *27*, 881–889. [CrossRef] [PubMed]
32. Vesnin, S.; Turnbull, A.K.; Dixon, J.M.; Goryanin, I. Modern Microwave Thermometry for Breast Cancer. *J. Mol. Imaging Dyn.* **2017**, *7*, 1000136
33. Polyakov, M. Cluster Analysis of the Results of Numerical Simulation of Thermometric Data. In Proceedings of the 2021 International Conference on Information Technology and Nanotechnology (ITNT), Samara, Russia, 20–24 September 2021; pp. 1–4.
34. Polyakov, M.; Khoperskov, A.; Emelyanov, E.; Borisovskii, E. The Using of Machine Learning and Neural Networks in the Processing of Computer Simulation Results for Medical Diagnostics. *CEUR Workshop Proc.* **2020**, *2667*, 189–192.
35. Särestöniemi, M.; Singh, D.; Dessai, R.; Heredia, C.; Myllymäki, S.; Myllylä, T. Realistic 3D Phantoms for Validation of Microwave Sensing in Health Monitoring Applications. *Sensors* **2024**, *24*, 1975. [CrossRef]
36. Flores, M.B.; Mourão, A.P.; del Rio, M.C. Breast Phantom Made of Acrylic Slabs for Tests in Mammography DR. *Appl. Radiat. Isot.* **2022**, *188*, 110389. [CrossRef] [PubMed]
37. Kabir, N.A.; Okoh, F.O.; Yusof, M.F.M. Radiological and Physical Properties of Tissue Equivalent Mammography Phantom: Characterization and Analysis Methods. *Radiat. Phys. Chem.* **2021**, *180*, 109271. [CrossRef]
38. Neira, L.M.; Mays, R.O.; Hagness, S.C. Human Breast Phantoms: Test Beds for the Development of Microwave Diagnostic and Therapeutic Technologies. *IEEE Pulse* **2017**, *8*, 66–70. [CrossRef]
39. Di Meo, S.; Pasotti, L.; Iliopoulos, I.; Pasian, M.; Ettorre, M.; Zhadobov, M.; Matrone, G. Tissue-Mimicking Materials for Breast Phantoms up to 50 GHz. *Phys. Med. Biol.* **2019**, *64*, 055006. [CrossRef]
40. Pollacco, D.A.; Conti, M.C.; Farrugia, L.; Wismayer, P.S.; Farina, L.; Sammut, C.V. Dielectric Properties of Muscle and Adipose Tissue-Mimicking Solutions for Microwave Medical Imaging Applications. *Phys. Med. Biol.* **2019**, *64*, 095009. [CrossRef]
41. Costanzo, S.; Cioffi, V.; Qureshi, A.M.; Borgia, A. Gel-Like Human Mimicking Phantoms: Realization Procedure, Dielectric Characterization and Experimental Validations on Microwave Wearable Body Sensors. *Biosensors* **2021**, *11*, 111. [CrossRef]
42. Castello-Palacios, S.; Garcia-Pardo, C.; Fornes-Leal, A.; Cardona, N.; Valles-Lluch, A. Tailor-Made Tissue Phantoms Based on Acetonitrile Solutions for Microwave Applications up to 18 GHz. *IEEE Trans. Microw. Theory Tech.* **2016**, *64*, 3987–3994. [CrossRef]
43. Valls-Esteve, A.; Tejo-Otero, A.; Adell-Gómez, N.; Lustig-Gainza, P.; Fenollosa-Artés, F.; Buj-Corral, I.; Rubio-Palau, J.; Munuera, J.; Krauel, L. Advanced Strategies for the Fabrication of Multi-Material Anatomical Models of Complex Pediatric Oncologic Cases. *Bioengineering* **2024**, *11*, 31. [CrossRef]
44. Guo, R.; Lu, G.; Qin, B.; Fei, B. Ultrasound Imaging Technologies for Breast Cancer Detection and Management: A Review. *Ultrasound Med. Biol.* **2018**, *44*, 37–70. [CrossRef] [PubMed]
45. Keenan, K.E.; Wilmes, L.J.; Aliu, S.O.; Newitt, D.C.; Jones, E.F.; Boss, M.A.; Stupic, K.F.; Russek, S.E.; Hylton, N.M. Design of a Breast Phantom for Quantitative MRI. *J. Magn. Reson. Imaging* **2016**, *44*, 610–619. [CrossRef]
46. Zhou, C.; Chase, J.G.; Ismail, H.; Signal, M.K.; Haggers, M.; Rodgers, G.W.; Pretty, C. Silicone Phantom Validation of Breast Cancer Tumor Detection Using Nominal Stiffness Identification in Digital Imaging Elasto-Tomography (DIET). *Biomed. Signal Process. Control* **2018**, *39*, 435–447. [CrossRef]
47. Martellosio, A.; Pasian, M.; Bozzi, M.; Perregrini, L.; Mazzanti, A.; Svelto, F.; Summers, P.E.; Renne, G.; Preda, L.; Bellomi, M. Dielectric Properties Characterization From 0.5 to 50 GHz of Breast Cancer Tissues. *IEEE Trans. Microw. Theory Tech.* **2017**, *65*, 998–1011. [CrossRef]
48. Kiarashi, N.; Nolte, A.C.; Sturgeon, G.M.; Segars, W.P.; Ghate, S.V.; Nolte, L.W.; Lo, J.Y. Development of Realistic Physical Breast Phantoms Matched to Virtual Breast Phantoms Based on Human Subject Data. *Med. Phys.* **2015**, *42*, 4116–4126. [CrossRef]
49. Joachimowicz, N.; Conessa, C.; Henriksson, T.; Duchêne, B. Breast Phantoms for Microwave Imaging. *IEEE Antennas Wirel. Propag. Lett.* **2014**, *13*, 1333–1336. [CrossRef]
50. Bliznakova, K. The Advent of Anthropomorphic Three-Dimensional Breast Phantoms for X-Ray Imaging. *Phys. Med.* **2020**, *79*, 145–161. [CrossRef]
51. Carton, A.K.; Bakic, P.; Ullberg, C.; Derand, H.; Maidment, A.D. Development of a Physical 3D Anthropomorphic Breast Phantom. *Med. Phys.* **2011**, *38*, 891–896. [CrossRef]
52. Shea, J.D.; Kosmas, P.; Hagness, S.C.; Van Veen, B.D. Three-Dimensional Microwave Imaging of Realistic Numerical Breast Phantoms via a Multiple-Frequency Inverse Scattering Technique. *Med. Phys.* **2010**, *37*, 4210–4226. [CrossRef] [PubMed]
53. Glick, S.J.; Ikejimba, L.C. Advances in Digital and Physical Anthropomorphic Breast Phantoms for X-Ray Imaging. *Med. Phys.* **2018**, *45*, e870–e885. [CrossRef]

54. Madsen, E.L.; Hobson, M.A.; Frank, G.R.; Shi, H.; Jiang, J.; Hall, T.J.; Weaver, J.B. Anthropomorphic Breast Phantoms for Testing Elastography Systems. *Ultrasound Med. Biol.* **2006**, *32*, 857–874. [CrossRef]
55. Zastrow, E.; Davis, S.K.; Lazebnik, M.; Kelcz, F.; Van Veen, B.D.; Hagness, S.C. Development of Anatomically Realistic Numerical Breast Phantoms with Accurate Dielectric Properties for Modeling Microwave Interactions with the Human Breast. *IEEE Trans. Biomed. Eng.* **2008**, *55*, 2792–2800. [CrossRef] [PubMed]
56. Islam, M.T.; Samsuzzaman, M.; Kibria, S.; Islam, M.T. Experimental Breast Phantoms for Estimation of Breast Tumor Using Microwave Imaging Systems. *IEEE Access* **2018**, *6*, 78587–78597. [CrossRef]
57. Klemm, M.; Leendertz, J.A.; Gibbins, D.; Craddock, I.J.; Preece, A.; Benjamin, R. Microwave Radar-Based Breast Cancer Detection: Imaging in Inhomogeneous Breast Phantoms. *IEEE Antennas Wirel. Propag. Lett.* **2009**, *8*, 1349–1352. [CrossRef]
58. Porter, E.; Fakhoury, J.; Oprisor, R.; Coates, M.; Popović, M. Improved Tissue Phantoms for Experimental Validation of Microwave Breast Cancer Detection. In Proceedings of the Fourth European Conference on Antennas and Propagation, Barcelona, Spain, 12–16 April 2010; pp. 1–5.
59. Sarno, A.; Valero, C.; Tucciariello, R.M.; Dukov, N.; Costa, P.R.; Tomal, A. Physical and Digital Phantoms for 2D and 3D X-Ray Breast Imaging: Review on the State-of-the-Art and Future Prospects. *Radiat. Phys. Chem.* **2023**, *204*, 110715. [CrossRef]
60. Li, C.M.; Segars, W.P.; Tourassi, G.D.; Boone, J.M.; Dobbins, J.T. Methodology for Generating a 3D Computerized Breast Phantom from Empirical Data. *Med. Phys.* **2009**, *36*, 3122–3131. [CrossRef]
61. Ikejimba, L.C.; Graff, C.G.; Rosenthal, S.; Badal, A.; Ghammraoui, B.; Lo, J.Y.; Glick, S.J. A Novel Physical Anthropomorphic Breast Phantom for 2D and 3D X-Ray Imaging. *Med. Phys.* **2017**, *44*, 407–416. [CrossRef]
62. Oliveira, B.L.; O'Loughlin, D.; O'Halloran, M.; Porter, E.; Glavin, M.; Jones, E. Microwave Breast Imaging: Experimental Tumour Phantoms for the Evaluation of New Breast Cancer Diagnosis Systems. *Biomed. Phys. Eng. Express* **2018**, *4*, 025036. [CrossRef]
63. He, Y.; Liu, Y.; Dyer, B.A.; Boone, J.M.; Liu, S.; Chen, T.; Qiu, J. 3D-Printed Breast Phantom for Multi-Purpose and Multi-Modality Imaging. *Quant. Imaging Med. Surg.* **2019**, *9*, 63. [CrossRef] [PubMed]
64. Biswas, S.K.; Banerjee, S.; Baker, G.W.; Kuo, C.-Y.; Chowdhury, I. The Mammary Gland: Basic Structure and Molecular Signaling during Development. *Int. J. Mol. Sci.* **2022**, *23*, 3883. [CrossRef] [PubMed]
65. Gautherie, M. Temperature and Blood Flow Patterns in Breast Cancer During Natural Evolution and Following Radiotherapy. *Prog. Clin. Biol. Res.* **1982**, *107*, 21–64.
66. Chen, H.; Wang, K.; Du, Z.; Liu, W.; Liu, Z. Predicting the thermophysical properties of skin tumor based on the surface temperature and deep learning. *Int. J. Heat Mass Transf.* **2021**, *180*, 121804. [CrossRef]
67. Bowman, H.; Cravalho, M.; Woods, M. Theory, Measurement, and Application of Thermal Properties of Biomaterials. *Annu. Rev. Biophys. Bioeng.* **1975**, *4*, 43–80. [CrossRef]
68. Iljaz, J.; Wrobel, L.C.; Hriberšek, M.; Marn, J. The use of Design of Experiments for steady-state and transient inverse melanoma detection problems. *Int. J. Therm. Sci.* **2019**, *135*, 256–275. [CrossRef]
69. Gordon, R.A.; Roemer, R.; Horvath, S. Mathematical Model of the Human Temperature Regulatory System— Transient Cold Exposure Response. *IEEE Trans. Biomed. Eng.* **1976**, *23*, 434–444. [CrossRef] [PubMed]
70. Gomboc, T.; Iljaz, J.; Wrobel, L.C.; Hribersek, M.; Marn, J. Design of constant temperature cooling device for melanoma screening by dynamic thermography. *Eng. Anal. Bound. Elem.* **2021**, *125*, 66–79. [CrossRef]
71. Sparks, J.L.; Vavalle, N.A.; Kasting, K.E.; Long, B.; Tanaka, M.L.; Sanger, P.A.; Schnell, K.; Conner-Kerr, T.A. Use of silicone materials to simulate tissue biomechanics as related to deep tissue injury. *Adv. Skin Wound Care* **2015**, *28*, 59–68. [CrossRef]
72. Dawson, C.A.; Visvader, J.E. The cellular organization of the mammary gland: Insights from microscopy. *J. Mammary Gland. Biol. Neoplasia* **2021**, *26*, 71–85. [CrossRef]
73. Anand, G.; Lowe, A.; Al-Jumaily, A. Tissue phantoms to mimic the dielectric properties of human forearm section for multi-frequency bioimpedance analysis at low frequencies. *Mater. Sci. Eng. Mater. Biol. Appl.* **2019**, *96*, 496–508. [CrossRef] [PubMed]
74. Liu, J.; Goehring, C.; Schiele, F.; Moeller, K.; Pott, P.P. Fabrication and Experimental Evaluation of Simple Tissue-Mimicking Phantoms with Realistic Electrical Properties for Impedance-Based Sensing. *Int. J. Integr. Eng.* **2021**, *13*, 127–136. [CrossRef]


**Disclaimer/Publisher's Note:** The statements, opinions and data contained in all publications are solely those of the individual author(s) and contributor(s) and not of MDPI and/or the editor(s). MDPI and/or the editor(s) disclaim responsibility for any injury to people or property resulting from any ideas, methods, instructions or products referred to in the content.